Dynamic Modeling and Input Shaping of Thermal Bimorph MEMS Actuators

Dan O. Popa[†], Byoung Hun Kang[†], John T. Wen[†],
Harry E. Stephanou[†], George Skidmore[‡], Aaron Geisberger[‡]

[†] Center for Automation Technologies, Rensselaer Polytechnic Institute,
Troy, New York, USA, e-mail: popa@cat.rpi.edu
[‡] Zyvex Corporation, Richardson, Texas, USA

Abstract

Thermal bimorphs are a popular actuation technology in MEMS (Micro-Electro-Mechanical Systems). Their operating principle is based on differential thermal expansion induced by Joule heating. Thermal bimorphs, and other thermal flexture actuators have been used in many applications, from micro-grippers, to micro-optical mirrors. In most cases open-loop control is used due to difficulties in fabricating positioning sensors together with actuator.

In this paper we present several methods for extracting reduced-order thermal flexture actuator models based on experimental data, physical principles, and FEA simulation. We then use the models to generate optimal driving signals using input shaping techniques. Both simulation and experimental results are included to illustrate the efficacy of our approach. This framework can also be applied to other types of MEMS actuators, including electrostatic comb drives.

1. Introduction

MEMS (Micro Electro-Mechanical Systems) technology is being increasingly used in micro-photonic, micro-fluidic, and RF commercial products. Over the last 15 years several actuation technologies at the micro-scale have gained wide acceptance, including piezo materials, shape memory alloys, thermal flexture actuators, and electrostatic comb drives [3,9]. Examples of such devices include micro-relays, micro-mirrors, and micro-grippers [9,11].

In most cases, closed-loop feedback control is not feasible for these devices due to the difficulty in integrating on-wafer position sensors. Capacitive position sensing can be used, but it requires fairly complex electronics, due to the very low capacitance ranges [12]. Without position feedback increased precision requirements on the thermal flextures can be addressed with greater quantitative analysis and modeling.

Previous modeling efforts for such micro-actuators include simplified PDE/ODE formulation from physical principles, finite element analysis, and reduced order modeling using Krylov subspace techniques [2,10,17,18]. Previous closed-loop control work is mostly based on external vision and laser-based position measurement [13]. In terms of open-loop control, finite element analysis together with direct experimentation have been used to generate driving signals [2,8].

Thermal micro-actuators can be fabricated in silicon together with other passive micro-components such as flexture joints, beams, and gears. Common fabrication techniques for Si thermal actuators include MUMPS surface micromachining, Sandia SUMMIT, and DRIE etching [3,5,6].

If the thermal bimorph actuators are used for the high-speed actuation of other MEMS structures, suppressing residual vibrations is highly desirable. Optical switching systems, for example, require the control of point-to-point motion of micro-mirrors used to redirect optical signals. Typical settling times are in the range of a few milliseconds [7]. Input shaping is a popular control method for vibration reduction, particularly well suited in applications where feedback signals are not available [14, 15]. In order to compensate for the absence of closed-loop control, an accurate plant model is required.

In this paper, we employ the following methodology for the synthesis of open-loop driving signals for thermal MEMS actuators: first, we derive ARX reduced order models based on a PDE approximation of the thermo-electro-mechanical behavior of the device; we then use the FEA model as a simulated plant for identifying the reduced order model; using this model, we generate a zero-vibration-derivative filter, and apply the shaped input back to the FEA simulation; we also apply the approach to actual experimental data; driving signals leading to the fastest output rise-time response in the presence of constraints are generated and experimentally tested using an optimization-based input-shaping technique, "output-matching"[16].

Although this paper focuses on thermal flexture actuators, a similar approach can be used to control more complex microstructures. This approach is especially useful for MEMS designers who currently invest a

considerable amount of experimentation time to find suitable driving signals for these actuators.

2. Thermal Bimorph Banks

The positioning accuracy, actuator bandwidth and force generated by thermal bimorph actuators, or actuator banks have been experimentally investigated in [1,2,3,4]. For thinner (2-4 μm) MUMPS bimorphs, bandwidths between 4 and 27 KHz, and displacements of up to 14 μm have been reported, depending on the geometry and number actuators, as well as on the environmental conditions. For thicker substrates, the force generated can be increased from a few μN to a few mN, while the bandwidth decreases to hundreds of Hz [1,2,3].

The geometry of basic thermal bimorph is shown in Figure 1(a). The basic structure has two beams called the "hot" and "cold" arms. The hot arm has a width of 8μm, about a third of the width of the cold arm. When a few volts are applied between the electrical pads, differential temperature profiles due to Joule heating produces a horizontal deflection. Using the basic bimorph structure, we can form actuator banks, as shown in Figure 1(b)-(e).

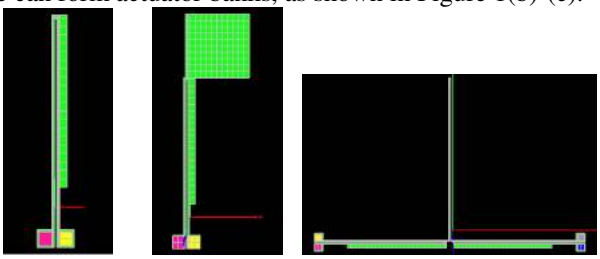

(a) 1 bimorph (b) Loaded bimorph (c) 2 bimorphs

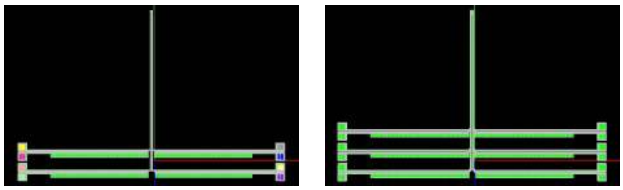

(d) 4 bimorphs (e) 6 bimorphs

Fig 1. Thermal bimorph structures. The basic structure (a) is 250 μm long, 3.5μm thick.

Figure 2 shows an example of a MUMPS rotary stage actuated by orthogonal banks of bimorphs. The angular velocity of the stage depends on the motion profile of each of the actuated arms and the size of the teeth.

3. Thermal Bimorph Modeling

Electrical current applied on the square contact pads provides the input for the thermal bimorph actuator. Its deflection is governed by thermal expansion resulting from heat dissipation, according to the heat equation written as:

$$\frac{dE}{dt} = W - H \,, E = cT \,, W = RI^2 \,. \qquad (1)$$

in which E is the thermal energy stored in the microstructure, W is the power generated by Joule heat, and H is the heat transferred to the environment and substrate.

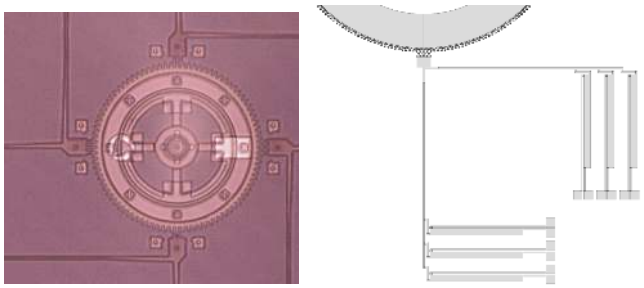

(a) (b)

Fig 2. Actual MUMPS rotary stage (a), using 4 orthogonal thermal bimorph banks (b).

$$\begin{aligned} H &= H_{convection} + H_{conduction} + H_{radiation} \\ H_{conduction} &= \lambda \Delta T, H_{radiation} = f(T^4) \\ H_{convection} &= KT + F(T_{air}, T_{substrate}) \end{aligned} \qquad (2)$$

In Eqns. (1) and (2) c is the volumetric specific heat coefficient, λ is the thermal conductivity and K is convection coefficient. Assuming the radiation term is negligible i.e., the hot arm does not reach very high temperatures, eqn. (1) can be rewritten in the form:

$$c\frac{\partial T(t,x)}{\partial t} = \lambda \frac{\partial^2 T(t,x)}{\partial x^2} + \frac{V(t)^2}{R(T(t,x\_),x)} - KT(t,x) \qquad (3)$$

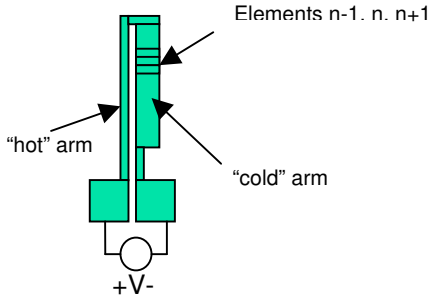

Fig 3. Discretized thermal bimorph

A spatial discretization as shown in Figure 3 leads to the finite element approximation model for the heat equation:

$$c_n \frac{dT_n(t)}{dt} = \lambda_{n1} T_n + \lambda_{n2} T_{n-1} + \lambda_{n3} T_{n+1} + \frac{R_n(T_n) V(t)^2}{\left(\sum_n R_n\right)^2} \qquad (4)$$

in which the resistance of the n-th element, Rn is temperature dependent:

$$R_n(T) = R_{no}(1 + \alpha_R T_n) \,. \qquad (5)$$

If $[\underline{x}]$ and $[\underline{T}]$ are column vectors representing the centroid positions, and temperatures of all the elements, the mechanical equations of motion for the device corresponding to the FEA model can be written as:

$$[M][\ddot{\underline{x}}] + [B][\dot{\underline{x}}] + K[\underline{x}] = [F], \quad (6)$$

where [*M*], [*B*], and [*K*] are the mass, damping and stiffness matrices, while the driving force for the system is generated by thermal expansion. Assuming a constant coefficient of thermal expansion, α, the actuator force at its tip element can be expressed as

$$[F] = \alpha[N][\underline{T}], \quad (7)$$

where [*N*] is a linear matrix linking the displacement of the actuator tip to small displacements of each element. The full dynamic model of the bimorph can now be expressed as:

$$[M][\ddot{\underline{x}}] + [B][\dot{\underline{x}}] + K[\underline{x}] = \alpha[N][\underline{T}]$$
$$[\dot{\underline{T}}] = [\Lambda][\underline{T}] + V^2(t)\ ([R_1] + R_2[\underline{T}]) \quad (8)$$

With the chain-connected elements in Figure 3, all the matrices in Equation (8) will be tri-diagonal. A typical FEA solver will integrate this equation over time to provide a solution. A modal analysis on the mechanical structure for 250 μm bimorphs reveals a dominant first mode along the Z axis (out of plane), and another along the X-axis (in-plane) as shown in Table 1.

Unit: Hz

Structure	Mode 1 (Z)	Mode 2 (X)	Mode 3 (X)
1 Bimorph	50,841.6	82,612.3	387,825
2 Bimorph	16,786.9	19,413.5	36,247.7
4 Bimorph	22,152.3	25,915.2	36,723.7
6 Bimorph	28,852.2	37,934.7	42,674.4
Load Mass	12,160.2	23,786.7	82,301.4

Table 1. Natural Frequencies of bimorph structures

We are primarily interested in the in-plane motion of the actuator (X), along which the excitation displacement occurs. As a first order approximation, we can retain the first order mode of the thermo-mechanical model using two characteristic arm temperatures (hot and cold):

$$m\ddot{x} + b\dot{x} + k\,x = \alpha N_1 T_{hot} + \alpha N_2 T_{cold}$$

$$\dot{T}_{cold} = \Lambda_{11} T_{cold} + \Lambda_{12} T_{hot} + (R_{11} + R_{211} T_{cold} + R_{212} T_{hot}) V^2$$
$$\dot{T}_{hot} = \Lambda_{21} T_{cold} + \Lambda_{22} T_{hot} + (R_{12} + R_{212} T_{cold} + R_{22} T_{hot}) V^2 \quad (9)$$

where x is now a scalar variable representing small displacements of the bimorph tip element along the X (horizontal) axis of motion.

If we time-discretized equation (9) with a sampling rate *Ts*, we obtain a difference equation with three states (x, T_{hot}, T_{cold}), one input (V), and one output (x):

$$x_k = a_1 x_{k-1} + a_2 x_{k-2} + c_1 T_{hot,k} + c_2 T_{cold,k}$$

$$T_{cold,k} = e_{11} T_{cold,k-1} + e_{12} T_{hot,k-1} + (f_{11} + g_{11} T_{cold,k-1} + g_{12} T_{hot,k-1}) V_{k-1}^2 \quad (10)$$

$$T_{hot,k} = e_{21} T_{cold,k-1} + e_{22} T_{hot,k-1} + (f_{21} + g_{21} T_{cold,k-1} + g_{22} T_{hot,k-1}) V_{k-1}^2$$

By eliminating the temperatures state in the discretized equation through back-substitution, and further assuming that the *g* coefficients are negligible, we obtain the following 3-rd order ARX model:

$$x_k + a_1 x_{k-1} + a_2 x_{k-2} + a_3 x_{k-3} = b_1 V_{k-1}^2 \quad (11)$$

3. Simulation Results

3.1 FEA Dynamic Simulation

For identification purposes, we use both trapezoid voltage inputs, as well as PRBS (Pseudo Random Binary Sequences) inputs, as shown in Figure 4. The trapezoidal ramps were selected such that the signal appears like a true step function through the first resonance mode, but it is much higher than the FEA time integration step (fixed at 1 μs).

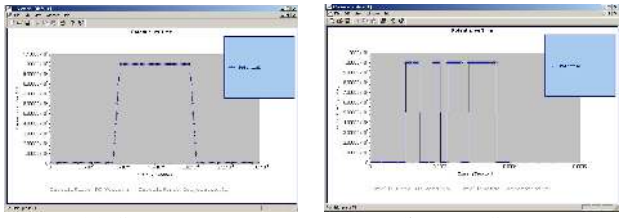

(a) Step Input (b) PRBS Input

Fig 4. Dynamic Inputs

The material constants used in the FEA model for the polysilicon MUMPS bimorphs are fairly well known, with the exception of thermal convection coefficients as well as the structural and air damping coefficients. Even though the selected values for our simulation may not be equal to actual values, the intent here was only to check the performance of the 3rd order modeling assumption. The FEA dynamic displacement response for the MEMS structures considered in this paper are shown in Figure 5. With an increased number of bimorphs, the deflection increases slightly, and the actuation force will increase significantly, although not linearly due to added stiffness.

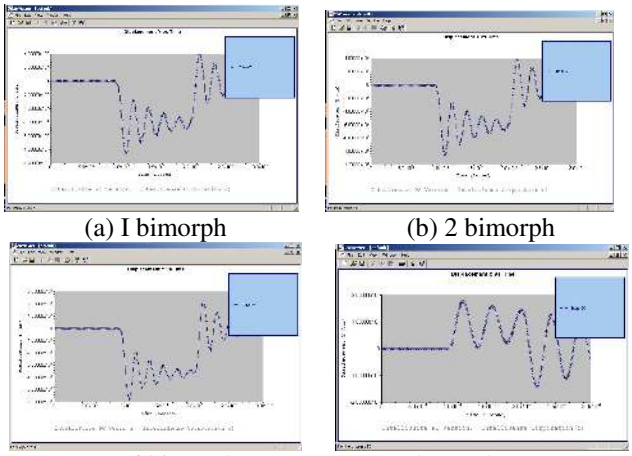

(a) I bimorph (b) 2 bimorph

(c) 6 bimorph (d) Load Mass

Fig 5. Dynamic step responses of MEMS structures

3.2 System ID on FEA simulated I/O data sets and input shaping

Although MEMS devices tend to have very small inertias, high-speed point-to-point motion, or actuator loading can result in significant vibration. Input shaping is a viable approach to shape the input command in order to reduce this vibration.

The fitted third order model for FEA displacement data was:

$$H_{sys} = \frac{0.0174}{z^3 - 1.737z^2 + 1.025z - 0.0748} \quad (12)$$

Figures 6 and 7 show the ARX identification results using both step and PRBS. In each case, using the fitted model we then apply a "zero-vibration-derivative" filter design [14,15] to generate voltage inputs. ZVD was chosen over a simpler ZV filter because of its better robustness. The original inputs (steps or PRBS) are then convolved with the shaping filters and applied back into the FEA models. The residual vibration are completely canceled by shaped inputs on the ARX model, but are still present in the FEA response due to modeling errors from nonlinear-effects.

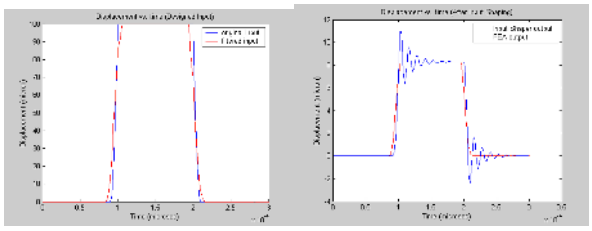

(a) Original and Shaped Input (b) FEA Output Response

Fig 6. Simulation Results for 1 bimorph actuator

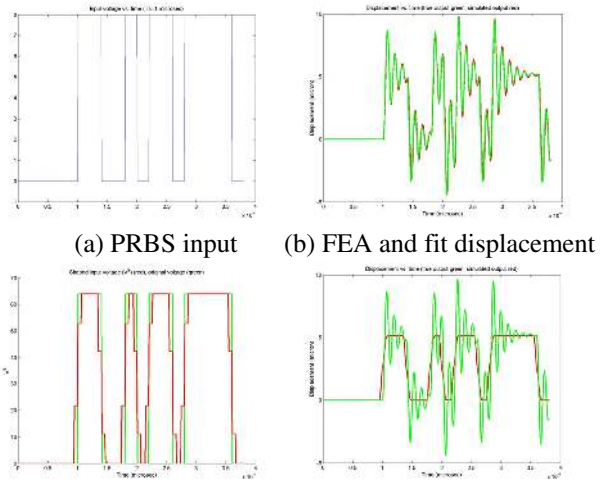

(a) PRBS input (b) FEA and fit displacement

(c) Shaped input (e) Shaped response

Fig 7. ZVD Input shaper using PRBS input

4. Experiments

4.1 Experimental Setup

Using a UMECH networked probe station instrumented with a stroboscopic, high-resolution camera, we performed transient displacement experiments on 3.5 μm thick, 250 μm long, single bimorph actuators (Figure 8). The probe station can sample displacement at arbitrarily sampling intervals as low as 0.1μs, by collecting video buffers of variable lengths from periodic inputs. In our experiments, however, we provided input signals sampled at 1μs, and recorded displacement data sampled at 10 μs and 33 μs. Based on repeated experiments on the same actuator, the actual measurement accuracy was estimated to be better than 2 μm and 0.5 μm, respectively, for total displacements of up to 8 μm.

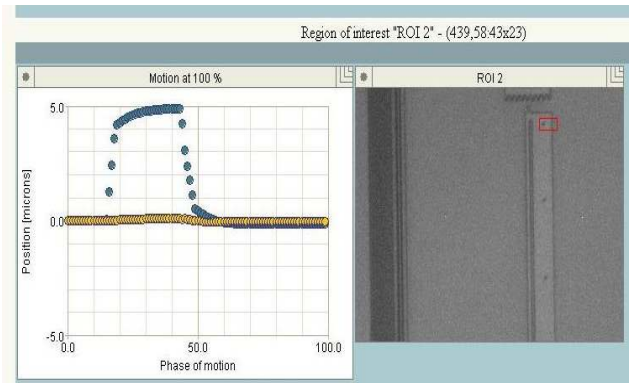

Fig 8 Experimental setup with one bimorph

Figure 9 shows a typical x displacement response by applying a step-input voltage. We noticed that the system has an over damped behavior and that the measured thermal bandwidth is much lower than predicted by our

FEA model. In fact, the thermal bandwidth of the actuator is 4.33 KHz, an order of magnitude lower than the first mechanical resonant mode. As a result, the system behaves essentially like a first order pole. In all the unloaded actuator cases considered in this paper, the thermal transient will dominate the first mechanical vibration. Therefore, in this case, ZVD filtering is not necessary, but we would like to decrease the response rise-time in the presence of input voltage saturation.

The first order model fit corresponding to experimental I/O data is:

$$G_p(s) = \frac{0.012s + 2538}{s + 27220}, X = G_p V^2 \quad (13)$$

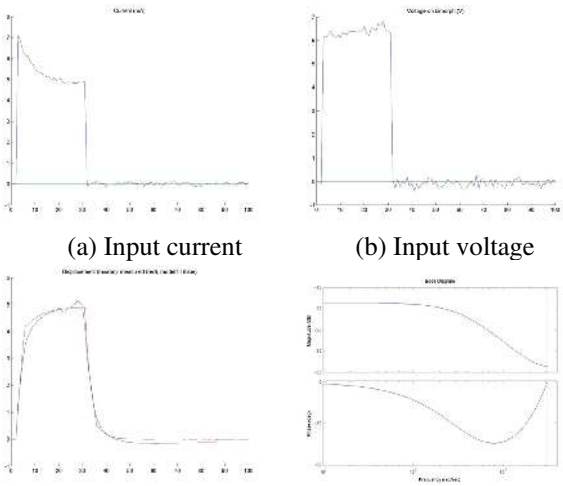

(a) Input current (b) Input voltage

(c) Displacement (d) Bode plot of fit

Fig 9: Experimental dynamic response of a single bimorph. (c) shows both the measured x displacement (noisy), and the model fit response (smooth).

4.2 Input shaping using the output matching method

Using this model, we pose the following constrained optimal control problem:

Given plant model G, and a desired output trajectory yd(t), find the optimal, constrained control input u(t) minimizing the 2-norm:

$$\min_{u \in L_2[0,T]} \| Gu - y_d \|_2, \max |u(t)| \le u_{\max} \quad (17)$$

In our case, an 8V maximum input voltage constraint was imposed, and the desired displacement profile for the thermal bimorph is a step as shown in Figure 10. A solution (Figure 11) using the output-matching method [16], can be obtained using with N=50 sinusoidal basis functions, and the constrained linear square nonlinear solver from the MATLAB optimization toolbox.

This optimal input profile is verified experimentally as shown in Figures 12 and 13. The fastest rise time with no overshoot corresponds to maintaining the input voltage at the maximum 8V for 4 μs. Maintaining it for 0-3 μs leads to a slower rise-time, and the 5 μs response exhibits overshoot.

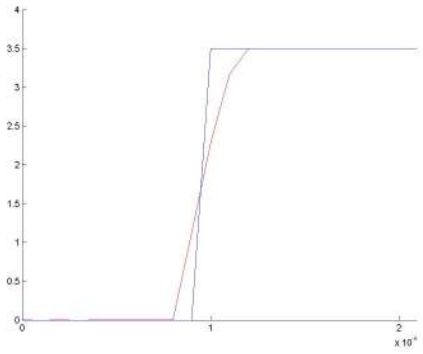

Fig 10: Desired bimorph displacement profile (fast), and simulated displacement profile using optimal input constrained solution using N=50 basis functions (slow).

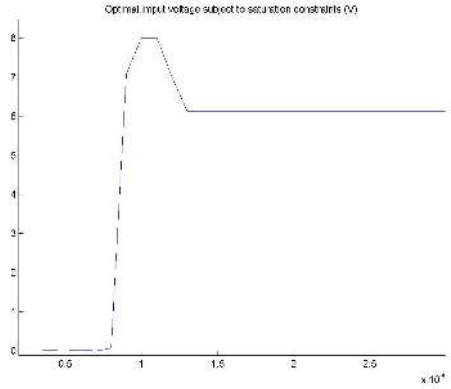

Fig 11: Optimal input profile with 8V maximum applied voltage constraint.

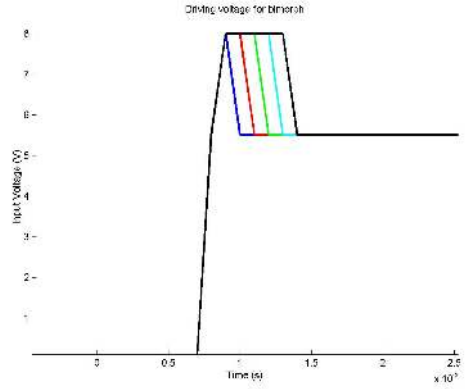

Fig 12: Experimental applied voltage input profiles.

5. Conclusion

In this paper we presented a model-based approach to generating optimal inputs for controlling displacement of thermal MEMS actuators. An open-loop approach is advantageous for these devices because of difficulties and cost of integrating on-wafer sensors.

We are currently applying this approach to other types of MEMS actuators under open loop control, such as electrostatic comb drives, MEMS micro-mirrors, and multi-degree of freedom microrobots.

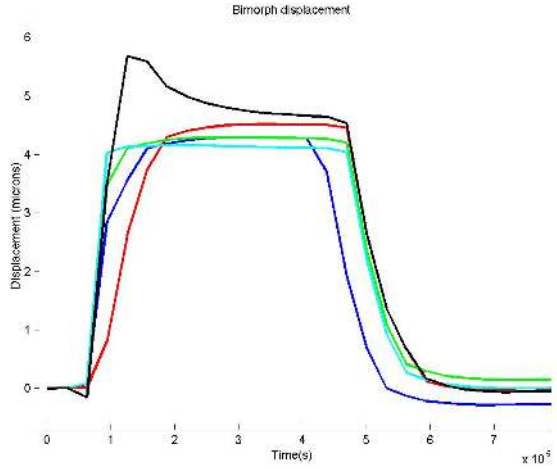

Fig 13: Measured bimorph tip displacements corresponding to applied voltages in Figure 12.

Acknowledgement

This work was performed under the support of the U.S. Department of Commerce, National Institute of Standards and Technology, Advanced Technology Program, Cooperative Agreement Number 70NANB1H3021. This research is supported in part by the National Science Foundation Grant CMS-0301827.

References

[1] J.H. Comtois, V.M. Bright, M.W. Phipps, "Thermal Microactuators for Surface Micro-machining Processes", *Proc. SPIE*, vol 2642, 1995, pp.10-21.

[2] D.M. Burans, V.M. Bright, "Design and performance of a double hot arm polysilicon thermal actuator", *Proc. of SPIE*, vol3224, 1997, pp.296-306.

[3] J.H. Comtois, M.A. Michalicek, C.C. Barron, "Fabrication Micro-Instruments in Surface-Micromachined Polycrystalline Silicon", *Proc. of the 43rd International Symposium Instrument Society of America*, 1997, pp.169-179.

[4] J. H. Comtois, V. M. Bright, "Design Techniques for Surface Micromachining MEMS Processes", *Proc. of SPIE, Micromachining and Microfabrication Process Technology*, vol2639, 1995, pp.211-222.

[5] K. W. Markus, D. A. Koester, A. Cowen, "MEMS Infrastructure: The Multi User MEMS Processes (MUMPs)", *Proc. of SPIE, Micromachining and Microfabrication Process Technology*, vol2639, 1995, pp.54-63.

[6] C.C. Barron, B.R. Davies, J. H. Comtois, "SAMPLE (Sandia Agile MEMS Prototyping, Layout tools, and Education)", Proc. of SPIE, *Micromachining and Microfabrication Process Technology III*, vol3223, 1997, pp.10-16.

[7] J. C. Chiou, Yu-Chen, Yi-Cheng Chang, "Dynamic Characteristics Measurement System for Optical Scanning Micromirror", *Proc. of SPIE, Micromachining and Microfabrication*, vol4230, 2000, pp.180-186.

[8] A. Q. Liu, X. M. Zhang, L. M. Lam, "A 4×4 MEMS Optical Cross-connectors (OXCs)", *Proc. of SPIE, Micromachining and Microfabrication*, vol4230, 2000, pp.174-179.

[9] M. Goldfarb, N. Celanovic, "Modeling Piezoelectric Stack Actuators for Control of Micromanipulation", *IEEE Control Systems Magazine*, June 1997, pp. 69-79.

[10] S. L. Miller, et. al., "Performance Tradeoffs for a Surface Micromachined Microengine*", Trans. Of SPIE*, vol. 2882, 1996, pp. 182-191.

[11] P.B. Chu and K.S.J. Pister, ``Analysis of Closed-loop Control of Parallel-Plate Electrostatic Microgrippers", *IEEE Intl. Conf. on Robotics and Automation*, San Diego, CA 1994, pp. 820-825.

[12] E.T. Enikov and B.J. Nelson, "Three Dimensional Microfabrication for Multi-Degree of Freedom Capacitive Force Sensor Using Fiber-Chip Coupling," *Journal of Micromechanics and Microengineering*, 10(4), pp. 492-497, Dec., 2000.

[13] Y. Zhou, B.J. Nelson, and B. Vikramaditya, "Integrating Optical Force Sensing and Visual Servoing for Microassembly," *Journal of Intelligent and Robotic Systems*, 28(3), pp. 259-276, July 2000.

[14] N.C. Singer, W.P. Seering, "Design and Comparison of Command Shaping Methods for Controlling Residue Vibrations", *IEEE Intl. Conf. on Robotics and Automation*, Scottsdale, AZ, 1989.

[15] W.E. Singhose, N.C. Singer, W.P. Seering, "Shaping Inputs to Reduce Vibration", *IEEE Intl. Conf. on Robotics and Automation*, Cincinatti, OH, 1990, pp. 922-927.

[16] J.T. Wen, B. Potsaid, "Input Shaping for Motion Control", CAT Report, Rensselaer Polytechnic Institute, May 2002.

[17] J.V. Clark, et.al,, "Addressing the Needs of Complex MEMS Design", Proc. IEEE International MEMS Conf., Las Vegas, NV, Jan. 20-24, 2002.

[18] N. Zhou, J. V. Clark, K. S. J. Pister, "Nodal Simulation for MEMS Design Using SUGAR v0.5." In *1998 International Conference on Modeling and Simulation of Microsystems Semiconductors, Sensors and Actuators* Santa Clara, CA, April 6-8, 1998, pp. 308-313.